Journal of Cleaner Production 389 (2023) 136071

Contents lists available at ScienceDirect

Journal of Cleaner Production

journal homepage: www.elsevier.com/locate/jclepro

Environmental life cycle assessment of wire arc additively manufactured steel structural components

Izhar Hussain Shah [a,1], Nicolas Hadjipantelis [b,1], Lulu Walter [c], Rupert J. Myers [a,*], Leroy Gardner [a,*]

[a] Department of Civil and Environmental Engineering, Imperial College London, Skempton Building, London, SW7 2AZ, UK
[b] Department of Civil and Environmental Engineering, University of Cyprus, 1 Panepistimiou Avenue, 2109, Nicosia, Cyprus
[c] Buro Happold, 17 Newman Street, London, W1T 1PD, UK

ARTICLE INFO

Handling Editor: Zhen Leng

Keywords:
Additive manufacturing
Life cycle assessment
Steel structures
Sustainability
Topology optimisation
Wire arc additive manufacturing

ABSTRACT

Wire arc additive manufacturing (WAAM) enables the production of structural components with topologically optimised geometries thus leading to significant self-weight reductions for a given load-carrying capacity. A common question arises regarding the environmental performance of WAAM structural components in comparison with conventional steel structural components. Thus, a comparative cradle-to-gate life cycle assessment has been conducted where the environmental impact of producing a topologically optimised WAAM steel beam is compared with that of producing a conventional hot-rolled steel I-beam. The beams are 2 m long, simply-supported and loaded vertically at midspan. The impact of using either carbon steel or stainless steel is investigated. The results demonstrate that the carbon steel and stainless steel WAAM beams have 7% and 24%, respectively, lower climate change impact than the corresponding I-beams. It is concluded that WAAM can lead to lower CO_2-eq. emissions than conventional hot-rolling, provided that mass reductions of the order of 50% (which are readily attainable) can be achieved by employing WAAM in conjunction with, for instance, topology optimisation. Furthermore, it is shown that the shielding gas contributes greatly to the environmental impact of WAAM, and that, by using higher deposition rates or by utilising renewable energy sources, the impact of WAAM can be reduced by more than 30%.

1. Introduction

Globally, the total CO_2 emissions attributed to the iron and steel sector in 2019 amounted to approximately 3.6 Gt, with the sector accounting for more than 8% of the total energy use (IEA, 2020). Each tonne of crude steel results in approximately two tonnes of total CO_2 emissions (IEA, 2020), of which 74%, 17% and 9%, respectively, correspond to the production, forming and fabrication of the final products (Allwood et al., 2010). With the aim to move the industry towards a 'net zero' future, interest has been growing for disruptive technologies that can reduce the environmental footprint of steel products and that can be implemented at the scale of the construction industry (Baumers et al., 2016).

Metal additive manufacturing, also referred to as metal 3D printing, is a rapidly evolving technology allowing the manufacture of geometrically complex and high-precision metal components that are not technologically or economically feasible with conventional shaping techniques, such as casting and forming (Gardner, 2023; Kanyilmaz et al., 2022; Liu et al., 2021; Tofail et al., 2018). Owing to the reduced wastage, easier customisation, higher material efficiency and shorted lead times it offers (Bekker and Verlinden, 2018; Ding et al., 2015; Huang et al., 2013; Wu et al., 2018b), metal additive manufacturing opens up a promising new path towards reducing the environmental impact of the steel sector.

Several metal additive manufacturing methods exist currently; those deemed most suitable for the construction industry are powder bed fusion and directed energy deposition (Buchanan and Gardner, 2019; Haghdadi et al., 2021), both of which involve the addition of metallic material in successive layers. In powder bed fusion, a layer of metallic powder is spread and, subsequently, selected regions are sintered, while,

* Corresponding author.
E-mail addresses: izhar88@hotmail.com (I.H. Shah), hadjipantelis.nicolas@ucy.ac.cy (N. Hadjipantelis), lulu.walter@burohappold.com (L. Walter), r.myers@imperial.ac.uk (R.J. Myers), leroy.gardner@imperial.ac.uk (L. Gardner).
[1] These authors contributed equally to this work.

https://doi.org/10.1016/j.jclepro.2023.136071
Received 24 October 2022; Received in revised form 6 January 2023; Accepted 15 January 2023
Available online 17 January 2023

in directed energy deposition, metal is deposited directly in its final location (Karunakaran et al., 2010). Wire arc additive manufacturing (WAAM) is a directed energy deposition method, which, as shown in Fig. 1(a), utilises a robotic arm, off-the-shelf arc welding equipment and metallic wire as feedstock to produce monolithic metallic parts through the deposition of weld material in a layer-by-layer fashion (Williams et al., 2016).

In comparison with other metal additive manufacturing methods, WAAM offers high deposition rates (Frazier, 2014; Singh et al., 2021; Williams et al., 2016) that can exceed 9.5 kg/h (Martina et al., 2019) and is considered a cost-effective method, especially for the production of components from expensive metals, such as titanium and nickel alloys (Ding et al., 2015; Wu et al., 2018a; Rodrigues et al., 2021; Rodrigues et al., 2002; Zuo et al., 2022), owing to the high material efficiency, low material costs (Williams et al., 2016) and low wastage it offers. Other metal additive manufacturing processes, such as powder bed fusion (Zhang et al., 2022), can offer greater geometrical refinement and hence greater degrees of optimisation than WAAM, but at smaller scales and lower build rates. Unlike most other metal additive manufacturing methods where the size of the produced part is confined by the size of the printing chamber, the ability of WAAM to produce large-scale objects makes it highly suitable for both off- and on-site applications in steel construction (Buchanan and Gardner, 2019). Most importantly, the geometric freedom offered by WAAM enables the production of structural components with topologically optimised geometries. To date, several topologically optimised structural components have been produced using WAAM – for instance, the topologically optimised trusses generated by Ye et al. (2021), an example of which is shown in Fig. 1(b), and the Takenaka Structural Steel Connector (MX3D, 2022), shown in Fig. 1(c). In both cases, significant reductions in material consumption were achieved. The epitome of the new opportunities offered by WAAM is the 10.5 m span MX3D Bridge (MX3D, 2022; New Scientist, 2021), shown in Fig. 1(d), which has recently been installed in central Amsterdam following a series of verification and simulations (Gardner et al., 2020; Hadjipantelis et al., 2020; Huang et al., 2022b; Kyvelou et al., 2020; Kyvelou et al., 2021; Kyvelou et al., 2022).

Even though WAAM is gaining interest rapidly owing to the benefits it can offer in construction applications in terms of scale, speed and cost (Gardner et al., 2020; Huang et al., 2022a), a common question arises regarding the environmental performance of WAAM compared to conventional steel manufacturing processes, such as hot-rolling. While WAAM enables the production of topologically optimised structural components leading to significant material savings, it also involves additional production stages, *e.g.* wire drawing and arc welding, and thus additional energy inputs relative to conventional production processes. Commonly asked questions are thus:

i. What are the environmental impacts of using WAAM in construction applications?
ii. How much material savings must be achieved in order for WAAM to have lower environmental impacts than conventional steel manufacturing?
iii. Which are the key parameters controlling the environmental performance of WAAM?

Hence, in order to answer the above questions, this work investigates WAAM from a life cycle environmental perspective and determines how its environmental performance compares with that of conventional methods used to produce steel structural components.

Only a few studies have assessed the environmental implications of using additive manufacturing technologies specifically in construction (Saade et al., 2020); such studies include the works of Agustí-Juan and Habert (2017), Agustí-Juan et al. (2017) and Esposito Corcione et al. (2018). However, all of these studies express the embodied carbon of

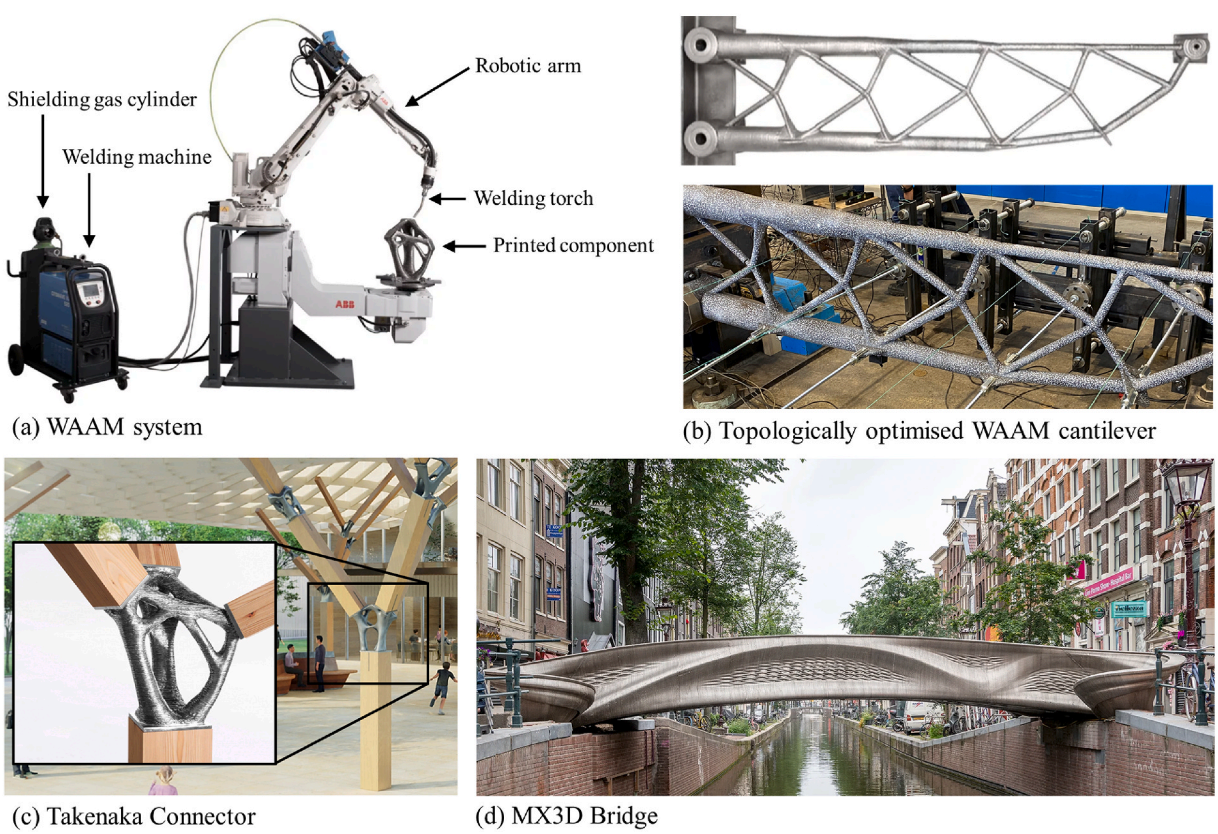

Fig. 1. (a) Principal components of a WAAM system. Examples of the application of WAAM in construction: (b) Topologically optimised WAAM cantilever under structural testing at Imperial College London; (c) The Takenaka Structural Steel Connector; (d) The MX3D Bridge in Amsterdam. Source: MX3D (2022).

structural elements per unit area – *i.e.*, a functional unit of m^2 was used, which is arguably a poor functional unit since it neglects structural properties (*e.g.* load-bearing resistance). Investigations that have studied the environmental impact of metal additive manufacturing in general include (Serres et al., 2011; Bourhis et al., 2013; Peng et al., 2017; Bekker and Verlinden, 2018; Liu et al., 2018; Priarone et al., 2018; Priarone et al., 2020; Campatelli et al., 2019; Dias et al., 2022; Kokare et al., 2023). However, only a handful of investigations have focused on the environmental performance of WAAM specifically. Campatelli et al. (2019) compared the total energy demand involved in an integrated additive-subtractive process, where WAAM is followed by a milling operation in order to achieve the desired surface finish, with that of a purely subtractive process (conventional milling) for the production of a single steel blade. The results demonstrated that the integrated additive-subtractive process can have a lower environmental impact than the purely subtractive process owing to the fact that the higher energy demand of the WAAM process can be compensated by the high material savings it offers in comparison with machining. By adapting the framework proposed by Priarone et al. (2019), Priarone et al. (2020) performed a cradle-to-gate life cycle assessment to compare the environmental impacts of three industrial WAAM components, namely an aerospace titanium bracket, a cantilever steel beam and an aerospace aluminium frame, when manufactured using a WAAM-based approach or using machining. It was concluded that the WAAM-based process can lead to sustantial reductions in energy usage and CO_2-eq. emissions and that the feedstock material production is the dominant contributor to its environmental impact. Dias et al. (2022) conducted a cradle-to-gate analysis to compare the environmental impact of using WAAM to produce a case study part in comparison with that of machining from solid. By considering ReCiPe endpoints, Dias et al. (2022) demonstrated that the benefit of using WAAM originates from the high material efficiency and low wastage it offers. Kokare et al. (2023) evaluated the environmental performance of WAAM by means of a cradle-to-gate life cycle assessment of a single steel wall. The environmental performance of WAAM was compared with that of laser powder bed fusion and computer numeric control (CNC) milling, demonstrating that, for the case of the studied steel wall, WAAM had a 55% higher environmental impact than CNC milling. However, it was suggested that, in the case of more complex geometries, such as the case studied in the present paper, WAAM can potentially have a lower environmental impact than CNC milling. Bekker and Verlinden (2018) conducted a cradle-to-gate life cycle assessment utilising a mass-based functional unit to compare the environmental impact (expressed in terms of ReCiPe midpoints and endpoints) of WAAM stainless steel with more conventional production techniques, such as green sand casting and CNC milling. Bekker and Verlinden (2018) concluded that (i) the environmental impact of WAAM is of similar scale to that of conventional manufacturing techniques, and that (ii) it is directly correlated to the mass of the product since the largest percentage of the environmental damage originates from the stainless steel itself. Hence, it was concluded that, through the application of topology optimisation, WAAM can offer opportunities for reductions in the environmental impact of steel components.

With the aim to investigate the environmental performance of WAAM in construction applications, the present study conducts, for the first time, a comparative environmental life cycle assessment of wire arc additively manufactured structural members and conventional hot-rolled structural members. In contrast with the aforementioned studies, which utilised either an area- or a mass-based functional unit, the present study takes into account the function and load-carrying capacity of the considered structural element (Purnell, 2012), by normalising the embodied carbon in the beam with respect to its load-carrying capacity for a given span. The life cycle performance of WAAM is assessed by comparing the environmental impact of the production process of a topologically optimised WAAM beam with that of a conventional hot-rolled steel I-beam, with the two beams having the same load-carrying capacity and span. A centrally loaded beam was chosen as the focus of the present study owing to its ubiquitous nature and general applicability across the construction industry. The environmental impact of using either carbon steel or stainless steel is investigated. Carbon steel was studied since it is the most widely used metallic structural material. Stainless steel was studied since, owing to its desirable durability, aesthetic appearance and structural properties, it has been gaining increasing usage over the last thirty years (Baddoo, 2008) in structural applications (Gardner, 2019), particularly in demanding environments. Further information on the use of stainless steel in construction is provided by Gardner (2005, 2008, 2019), Baddoo (2008) and Walport et al. (2022). In the last twenty years, the behaviour and design of stainless steel I-section structural members, such as that studied herein, has been investigated extensively – recent studies include those by Bu and Gardner (2018, 2019), Kucukler et al. (2020), dos Santos and Gardner (2020), Yang et al. (2019) and Xing et al. (2021).

This paper presents a cradle-to-gate life cycle assessment to investigate the environmental impact of producing (i) a carbon steel I-beam, (ii) a topologically optimised carbon steel WAAM beam, (iii) a stainless steel I-beam, and (iv) a topologically optimised stainless steel WAAM beam. Following the description of the adopted methodology, the results corresponding to eighteen midpoint impact categories, which represent different types of environmental issues, are reported and analysed. Comparisons between the four studied cases are made and conclusions regarding the influence of key parameters on the environmental performance of WAAM are drawn. Specifically, the influences of mass savings, deposition rate and electricity mix are investigated.

2. Methodology

2.1. Functional unit

Conventional steel production is represented by a standardised hot-rolled UB 203 × 133 × 25 prismatic I-section beam (British Steel, 2018), as shown in Fig. 2(a), referred to as the 'I-beam' herein. WAAM is represented by the topologically optimised truss shown in Fig. 2(b) and referred to as the 'WAAM beam' herein. The WAAM beam comprises circular tubular cross-sections of variable thickness and diameter and has been generated by Ye et al. (2021), who developed an automated

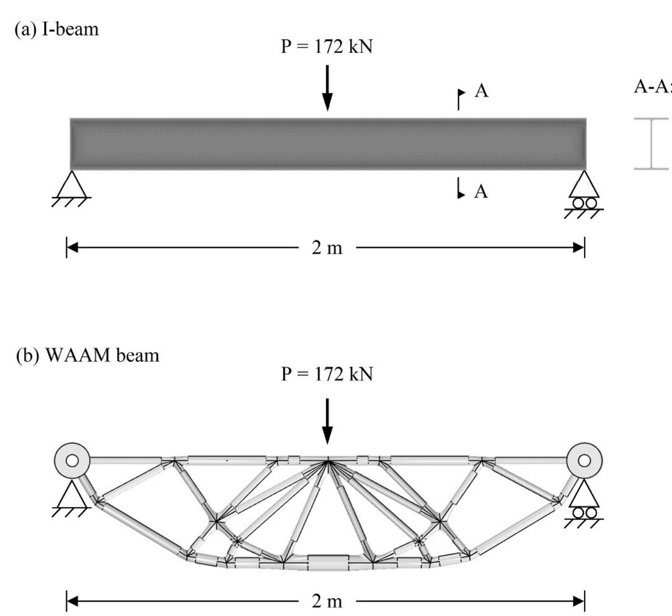

Fig. 2. (a) Conventionally produced steel I-beam and (b) topologically optimised WAAM beam (Ye et al., 2021) with the same span (2 m) and target load (172 kN).

end-to-end framework that combines optimisation techniques and WAAM to design and produce high-performance additively manufactured structures. The geometry of the WAAM beam was obtained through a numerical layout and geometry optimisation technique considering practical and manufacturing constraints, as well as a 400 × 2000 mm design domain, simply-supported boundary conditions and vertical downwards loading at midspan. The topologically optimised WAAM beams, including the simply-supported beam studied herein, have been produced by MX3D (2022) as specimens for an experimental programme conducted at Imperial College London; the optimised WAAM cantilever is shown in Fig. 1(b).

Both beams are 2 m long, simply-supported and carry a vertical design load P at midspan. As frequently the case in floor and roof systems, it is assumed that sufficient lateral restraint is provided to the beams, such that no out-of-plane deformations can occur; *i.e.*, lateral torsional buckling is prevented and thus the design is governed by the in-plane bending capacity of the beams. As discussed by Ye et al. (2021), the two chosen beams can achieve the same target load $P = 172$ kN and thus have the same bending moment capacity. The geometry of the WAAM beam was defined by means of a topology optimisation process (Ye et al., 2021), by which the WAAM material was placed at the locations where it is more effective. As a result, the WAAM beam is 53% lighter than the I-beam. Specifically, the mass of the I-beam and WAAM beam is 50.2 kg and 23.6 kg, respectively; *i.e.*, the WAAM beam has a capacity-to-mass ratio that is 2.13 times that of the I-beam (Ye et al., 2021). Similar ratios were determined by Bruggi et al. (2021) and Laghi et al. (2022).

The functional unit is a steel beam of 2 m span and target load of $P = 172$ kN applied vertically downwards at midspan. Since the I-beam and WAAM beam have the same span and load-carrying capacity, the functional unit caters for both length and strength requirements (Purnell, 2012), thus making direct comparisons between the two beams realistic and relevant to industrial applications. Furthermore, the environmental impacts associated with using two different steel alloys, namely carbon steel (modelled as Grade S355) and stainless steel (modelled as austenitic Grade 304), are examined. This is performed for both the I-beam and the WAAM beam; hence, in total, four different inventory analysis models are developed herein.

2.2. System boundaries

A cradle-to-gate analysis has been conducted for the purposes of the present study, *i.e.*, the system boundaries included processes from material production to the completion of the product manufacture, which was assumed to take place in the United Kingdom. Hence, the production and maintenance of machinery and equipment, the collection and transport of steel scrap, all the steps following manufacturing, such as the transportation of the products from the factory to the end user, and the maintenance and end-of-life management of the beams were not part of the analysis. Four product systems were considered herein, as shown in Fig. 3(a)–(d). As described in more detail below, the production of the I-beams includes the unit processes of steel production, hot-rolling, fabrication and finishing, while the unit processes for the production of the WAAM beams include additionally the unit processes of wire drawing and WAAM printing.

2.3. Inventory analysis and modelling approach

The analysis was conducted using the OpenLCA software (GreenDelta, 2020), while the ecoinvent database v3.4 (ecoinvent, 2020) was utilised for the steel production, hot-rolling, wire drawing and welding processes. Direct inputs in the WAAM process included the metallic wire, shielding gas, and electric power, while outputs included welding spatter, welding fumes and the produced WAAM beam. Electricity consumption was modelled based on the electricity mix in the United Kingdom as of September 2021, comprising 42% natural gas, 18% wind, 16% nuclear, 10% imports, 5% solar, 5% biomass, 2% coal, 1% hydro and 1% storage (National Grid, 2021). The modelling approach adopted for each unit process is described in the following sub-sections.

2.3.1. Steel production and hot-rolling

The steel production process is common to all four cases and includes raw material extraction and preparation, reduction of iron ore to liquid iron in a furnace, introduction of oxygen and recycled scrap steel,

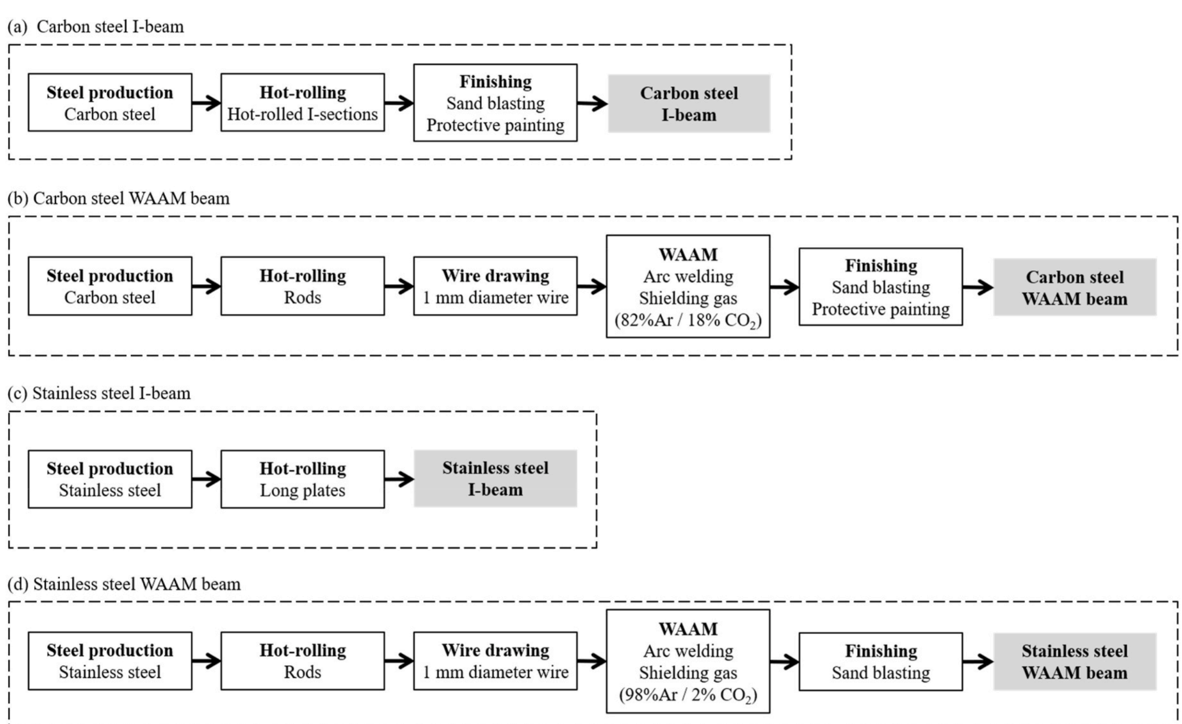

Fig. 3. System boundary and unit processes considered in the production of the I-beam and the WAAM beam; the black arrows represent the reference flows.

introduction of additives to form the desired steel grade, and continuous casting. In the developed models, carbon steel was modelled based on the ecoinvent process 'market for steel, unalloyed' and stainless steel was modelled based on the ecoinvent process 'market for steel, chromium 18/8'; the processes adopt chemical compositions that are similar to steel S355 grade and 304 stainless steel, respectively, which are widely used in construction. Following the production of both carbon steel and stainless steel, hot-rolling was modelled as a separate unit process based on the ecoinvent process 'hot-rolling, steel'.

2.3.2. Production of I-beams

In contrast to carbon steel I-beams, which are typically rolled from steel blooms, stainless steel I-beams are typically fabricated through the welding of individual plates. Standard Metal Inert Gas (MIG) welding has been assumed herein. The production of the carbon steel I-beam included sand blasting, which is required to clean the surface of the beam, and protective painting, which is required to provide corrosion protection. Sand blasting was modelled using the process 'fine machining' based on CES Edupack 2019 data (Granta Design, 2019), while the protective painting process was modelled based on the ecoinvent process 'solvent-borne alkyd paint'. Sand blasting and protective painting were assumed only for the carbon steel beam.

2.3.3. Production of WAAM beams

The raw material for WAAM is standard welding wire. The wire is produced using wire drawing which is a metalworking process where the cross-section of a steel rod is gradually reduced through a series of drawing dies. For both the carbon steel and stainless steel welding wire, drawing was modelled using the ecoinvent unit process 'wire drawing, steel', assuming a wire rod of diameter ranging between 5.5 mm and 16 mm being drawn to 1.0 mm diameter wire.

In WAAM printing, welding is used in conjunction with a robotic arm to deposit the metallic material in a layer-upon-layer fashion. For the purposes of the present study, welding was modelled manually assuming a deposition rate of 2 kg/h, which is at the upper end of the range of deposition rates utilised during the printing of the MX3D Bridge (Gardner et al., 2020). As described in detail in Section 4.2, for a deposition rate of 2 kg/h, the energy consumed by the welding process per kilogram of printed material has been taken as 1.97 kWh. Note that the interlayer dwell time (*i.e.,* the time period between layers during which the welding machine is idle until the previously deposited layer has cooled down to the chosen interpass temperature) is not considered herein; compared to the power consumption of the welding process, the idle state power consumption is typically negligible – for instance, the idle state power consumption of a Fronius TPS 500i power source, often used in WAAM, is 34.1W (Fronius International GmbH, 2022), which is less than 2% of the power consumption of the welding process modelled herein. Also note that the idle time can be minimized by printing multiple components in parallel. According to Bekker and Verlinden (2018), who performed empirical on-site measurements at the facilities of MX3D (2022), the energy consumptions associated with the robot movement and ventilation processes to produce 1 kg of steel at a deposition rate of 1 kg/h were 0.44 kWh and 0.54 kWh, respectively. Since a deposition rate of 2 kg/h was used herein (i.e. double the deposition rate studied by Bekker and Verlinden (2018)), the consumptions corresponding to the robot movement and ventilation were halved to 0.22 and 0.27 kWh per kilogram of printed material, respectively. Hence, the total energy consumption of the WAAM process has been taken as 2.46 kWh per kilogram of printed material. Note that, following the modelling approach of Bekker and Verlinden (2018), the environmental impact of the fumes emitted during the welding process were taken into account using the values from the 'welding arc steel' ecoinvent process.

The WAAM welding process requires the utilisation of shielding gas for the protection of the weld from atmospheric oxygen and moisture. In the case of carbon steel, an 82% argon and 18% CO_2 gas mixture was utilised, while, in the case of stainless steel, a 98% argon and 2% CO_2 gas mixture was utilised. The shielding gas mixtures were modelled using the 'market for carbon dioxide, liquid' and 'market for argon, liquid' unit processes, assuming a flow rate of 12 L/min. In the case of carbon steel, this corresponds to 0.517 kg of Argon and 0.114 kg of CO_2 per kilogram of printed material. In the case of stainless steel, it corresponds to 0.622 kg of Argon and 0.013 kg of CO_2 per kilogram of printed material. Argon, which is the major component of the shielding gases, is extracted from liquid air in a cryogenic air separation unit by means of fractional distillation. Argon is recovered and typically stored, handled and transported in liquid state, as opposed to compressed argon gas used in the actual welding process. In the present study, argon has been modelled in its liquid state and the impact of the upstream production processes, such as the cryogenic air separation, which requires significant energy inputs, has been taken into account. Additional processes, such as vaporisation, have been assumed to have a minimal impact on the results, and are excluded.

Sand blasting was assumed for both the carbon steel and stainless steel WAAM beams, however, protective painting was assumed only for the carbon steel WAAM beam.

2.3.4. Material utilisation fraction

The material utilisation fraction, which indicates the amount of material input carried forward in each of the proceeding unit processes after adjusting for waste and losses, is important in multi-step processes, such as the production of steel members. In the case of the I-beams, a material utilisation fraction of 1.0 was assumed for steel production, implying that material losses during continuous casting are negligible. Hot-rolling was assigned a material utilisation fraction of 0.96, taken as the average of the values reported in CES Edu (Granta Design, 2019), ecoinvent (2020), and Rentz et al. (1999), *i.e.*, 0.9–1.0, 0.95 and 0.94–0.99, respectively. Sand blasting was assumed to have a material utilisation fraction of 0.99, accounting for the removal of some material from the beam surface. Protective painting was given a material utilisation fraction of 1.0 since no material is lost during this step. As shown in Table A1 in Appendix A, the material fractions translate into an input mass of 1.04 kg per kilogram of produced I-beam – *i.e.*, 52.21 kg are required to produce the 50.2 kg I-beam.

In the case of the WAAM beams, as shown in Table A1 in Appendix A, steel production and hot-rolling were given the same material utilisation fractions as in the case of the I-beams. In wire drawing, material losses occur during the descaling process, with additional losses resulting from cutting scrap and dust. Large variations are reported in the literature regarding the amount of waste and losses during wire drawing. Based on CES Edu (Granta Design, 2019) and ecoinvent (2020), which report fractions of 0.85–0.9 and 0.96, respectively, a material utilisation fraction of 0.90 was assumed herein. Welding in WAAM was assigned a material utilisation fraction of 0.99, accounting for material losses due to welding spatter and cut wire (Bekker and Verlinden, 2018). An as-built surface finish has been assumed for the WAAM beams; in comparison with mechanical and aerospace parts, in construction, relatively high geometric tolerances are acceptable and fatigue is often not a critical design consideration, thus machining operations to smoothen the WAAM surface are typically not required – see, for instance, the examples of the application of WAAM in construction in Fig. 1(b)–(d). As shown in Table A1 in Appendix A, the material fractions translate into an input mass of 1.18 kg per kilogram of produced WAAM beam; *i.e.*, 27.85 kg are required to produce the 23.6 kg WAAM beam.

2.4. Impact assessment

In the present study, the ReCiPe 2016 method at midpoint level (following a 'hierarchist' interpretation) – a popular method in the additive manufacturing literature (Saade et al., 2020) – was used for the life cycle impact assessment. Midpoint results represent potential environmental impacts and form the main emphasis of this study, whereas endpoint results characterise damage to areas of protection at a more aggregated level (*i.e.*, human health, ecosystem and resources) (Kalbar et al., 2018). Eighteen midpoint impact categories are reported herein (Table 1).

In the present study, economic allocation was used, by which burdens were distributed depending on the revenues of co-products, by means of allocation factors from the ecoinvent database and literature. A cut-off approach was applied to deal with recycled by-products, allocating the production of material to the primary (upstream) user of the material. Hence, the benefits of recyclable products were not seen by the primary user (*e.g.*, steel producer) but instead came burden-free to the secondary user (*e.g.*, users of the recycled products) (ecoinvent, 2020; GreenDelta, 2020).

3. Results and analysis

3.1. Overall results

Results for the four beam types considered herein, *i.e.* the (1) carbon steel I-beam, (2) carbon steel WAAM beam, (3) stainless steel I-beam and (4) stainless steel WAAM beam, are presented in this section. The ReCiPe midpoint indicator values for all four beam types are shown in Table 1, where it is observed that the carbon steel I-beam has higher impact than the carbon steel WAAM beam in eight out of eighteen impact categories, including climate change and metal depletion. The carbon steel I-beam is nearly twice as impactful as the carbon steel WAAM beam in the metal depletion category; this is attributed to the high (53%) material savings achieved in the case of the WAAM beam by means of topological optimisation. The stainless steel I-beam has a higher impact than the stainless steel WAAM beam in thirteen out of eighteen impact categories, including climate change, fossil depletion and metal depletion, as well as in most of the toxicity categories.

As shown in Table 1, in the majority of categories, the stainless steel beams were found to have higher environmental impacts when compared with their carbon steel counterparts. This is attributed primarily to the contribution of the chromium and nickel elements in the production of stainless steel (Bekker and Verlinden, 2018; Ibbotson and Kara, 2013). This contribution is reflected clearly in the categories of metal depletion and toxicity (*e.g.*, freshwater, marine, and human toxicity). The higher environmental impact of stainless steel, however, must be weighed against the long-term benefits it offers (Purnell, 2012), such as corrosion resistance (Baddoo, 2008; Gardner, 2019), which leads to lower maintenance requirements and longer design lives (Gardner et al., 2007), however, these are not captured by the cradle-to-gate analysis conducted herein.

3.2. Contributions of unit processes

The contributions of the individual processes to climate change are listed in Table 2. In the production of the I-beams, the contribution of the steel production process to the total impact is 85% and 97% for the carbon steel and stainless steel cases, respectively. Thus, from the perspective of climate change, reducing the mass of the steel required for a given design capacity would be highly beneficial. As demonstrated in the present study, this can be achieved by combining topology optimisation, which seeks to minimise the amount of material for a given demand, with the WAAM technology, which enables the production of geometrically complex structural components. Specifically, as shown in Table 2, the impact of steel production in the case of the topologically optimised WAAM beams is 56% and 49% lower than that of the carbon steel and stainless steel I-beams, respectively. In the production of the carbon steel WAAM beam, the contribution of steel production to the total impact is 41%, which is similar to the 45% and 35% contributions reported by Kokare et al. (2023) and Priarone et al. (2020), respectively. The contribution of steel production to climate change can be reduced further by increasing the share of recycled scrap steel in the raw material mixture relative to primary ore-based steel. It is worth noting that the hot-rolling and protective painting (for carbon steel) processes have small but non-negligible contributions to the impacts of the I-beams.

As shown in Table 2, in the climate change impact category, the carbon steel WAAM beam has been found to be 7% less impactful than the carbon steel I-beam, with the WAAM process contributing more than steel production to the total impact (50% specifically), thus offsetting the entire (99%) reduction in the impact of steel production that was achieved through topology optimisation. In the case of the stainless steel beams, the WAAM beam was found to be 24% less impactful than the corresponding I-beam in the climate change category. In this case, the contribution of the WAAM process to the total climate change impact score is lower (32% specifically), offsetting a smaller proportion (49%) of the reduction in the impact of steel production that was achieved through topology optimisation.

The contributing elements to the environmental impact of the WAAM process are: (i) the electricity enabling the arc welding process, (ii) the shielding gas comprising argon and carbon dioxide (the specific ratio depends on whether carbon or stainless steel is welded) and (iii) the energy required for the production of the electronics of the WAAM system. As shown in Fig. 4, the use of shielding gas – mainly argon – has

Table 1
ReCiPe 2016 midpoint impact results [a], [b].

Impact category	Unit	Carbon steel I-beam	Carbon steel WAAM beam	Stainless steel I-beam	Stainless steel WAAM beam
Agricultural land occupation	m^2a	**0.197**	0.196	0.107	0.170
Climate change (GWP100)[c]	kg CO_2-eq.	**117**	109	248	190
Fossil depletion	kg oil-eq.	31.3	**31.4**	65.0	52.7
Freshwater ecotoxicity	kg 1,4-DCB-eq.	1.28	**1.66**	19.6	11.0
Freshwater eutrophication	kg P-eq.	0.0537	**0.0598**	0.0970	0.0869
Human toxicity	kg 1,4-DCB-eq.	38.3	**64.5**	149	124
Ionising radiation	kBq U_{235}-eq.	6.74	**25.5**	17.1	30.8
Marine ecotoxicity	kg 1,4-DCB-eq.	1.23	**2.07**	20.2	11.7
Marine eutrophication	kg N-eq.	0.132	**0.229**	0.297	0.320
Metal depletion	kg Fe-eq.	**65.3**	34.8	467	249
Natural land transformation	m^2	**0.0371**	0.0199	4.80×10^{-4}	2.75×10^{-3}
Ozone depletion	kg CFC-11-eq.	7.57×10^{-6}	$\mathbf{8.45 \times 10^{-6}}$	1.30×10^{-5}	1.19×10^{-5}
Particulate matter	kg PM_{10}-eq.	**0.433**	0.362	1.29	0.839
Photochemical oxidant	kg NMVOC	**0.579**	0.403	0.933	0.633
Terrestrial acidification	kg SO_2-eq.	**0.516**	0.433	1.24	0.855
Terrestrial ecotoxicity	kg 1,4-DCB-eq.	0.0781	**0.101**	0.0375	0.0871
Urban land occupation	m^2a	**1.09**	0.741	3.18	1.90
Water depletion	m^3	0.367	**0.493**	0.742	0.723

[a] Values in **bold** show the highest impact when comparing the carbon steel I-beam and WAAM beam.
[b] Underlined values show the highest impact when comparing the stainless steel I-beam and WAAM beam.
[c] Reported using global warming potential over a 100-year horizon (GWP100).

Table 2
Contribution of production processes to climate change (GWP100).

Process	Carbon steel I-beam (kg CO_2-eq.)	Carbon steel WAAM beam (kg CO_2-eq.)	Stainless steel I-beam (kg CO_2-eq.)	Stainless steel WAAM beam (kg CO_2-eq.)
Steel production	99.7	44.3	241	124
Hot-rolling	6.96	3.10	6.99	3.53
Wire drawing	–	1.94	–	2.18
WAAM	–	54.8	–	59.7
Sand blasting	0.248	0.117	–	0.241
Protective painting	10.6	4.96	–	–
Total impact	117	109	248	190

the greatest impact across several impact categories. In the case of climate change, the use of shielding gas accounts for 60% of the total impact, while the electricity utilised for the welding process accounts for 36%. The impact of argon gas is driven primarily by the highly energy-demanding processes involved in its own production, as discussed in Section 2.3.3. Hence, as discussed in Section 4.3, the electricity mix is important for both the power consumed for arc welding but also for the production of the shielding gas; potentially, utilising renewable energy sources can mitigate the environmental impacts of both the welding process and shielding gas production.

As investigated further in Section 4.2, the contribution of shielding gas, which is used at a fixed flow rate typically between 12 and 18 L/min, in the environmental impact of the WAAM process can be reduced significantly by increasing the deposition rate of the weld material (Bekker and Verlinden, 2018) – *e.g.* the volume of the consumed shielding gas can be halved by doubling the deposition rate. Note that a higher deposition rate would also reduce the power consumed for fume extraction. There is, however, a trade-off between deposition rate and printing quality, which is the subject of ongoing research.

It should be noted that the electricity consumed for welding is also influenced by the energy efficiency of the welding machine and by the waveform of the welding process; for instance, pulse arc welding, where amperage is fluctuated between high and low points and which has been assumed herein, is more energy efficient than non-pulsed arc welding. Lastly, all the aforementioned contributions would be reduced further if higher mass savings could be achieved through topology optimisation. A sensitivity analysis has been conducted to investigate the most significant considerations introduced above; the results are discussed in the following section.

4. Influence of key WAAM parameters

4.1. Influence of mass reduction

The results presented in Section 3 correspond to the case where the mass ratio between the I-beam and the WAAM beam is 2.13. As discussed in Section 2.1, this ratio resulted from a 53% mass reduction achieved in the case of the WAAM beam through topology optimisation (Ye et al., 2021). However, the achieved mass reductions can vary significantly depending on the chosen design parameters. For instance, under different end support and loading conditions, the optimisation procedure would provide a different optimal solution for the topology of the beam. Indicatively, in the case of a cantilever beam (shown in Fig. 1 (b)) subjected to a target edge load of 98 kN, Ye et al. (2021) reported an I-beam to WAAM beam mass ratio of 2.24, which is higher than the mass ratio in the case of the simply-supported beam studied herein. To investigate the influence of the degree of mass reduction on the key environmental impact categories, four additional analyses have been conducted, where the mass of the WAAM beam was defined hypothetically as 12.6 kg, 16.7 kg, 33.5 kg, and 50.2 kg. These mass values correspond to steel I-beam to WAAM beam mass ratios of 4:1, 3:1, 1.5:1 and 1:1, and thus mass savings of 75%, 67%, 33% and 0%, respectively.

The results corresponding to the impact categories of climate change, human toxicity and metal depletion in the case of the carbon steel beams are shown in Fig. 5. The results for all categories and for the stainless steel case are given in Appendix A, Table A3. As expected, in all categories, the higher the mass reduction (*i.e.*, the higher the I-beam to WAAM beam mass ratio), the lower the environmental impact of the WAAM beam relative to the I-beam. In the climate change impact category, a break-even point at an I-beam to WAAM beam mass ratio of 2:1 is identified, leading to the conclusion that, for a deposition rate of 2 kg/h, WAAM can lead to lower CO_2-eq. emissions than conventional hot-rolling when at least 50% mass savings can be achieved. In the cases of human toxicity and metal depletion, the break-even points are at mass ratios of 3.7:1 and 1.2:1, respectively, beyond which WAAM results in relatively lower impacts.

4.2. Influence of deposition rate

As discussed in Section 3.2, the environmental impact of the WAAM process is highly dependent on the deposition rate of the weld material. Thus, the influence of the deposition rate on the environmental impact of the WAAM process has been investigated by modelling (in addition to the 2 kg/h case presented in previous sections) the scenarios where the

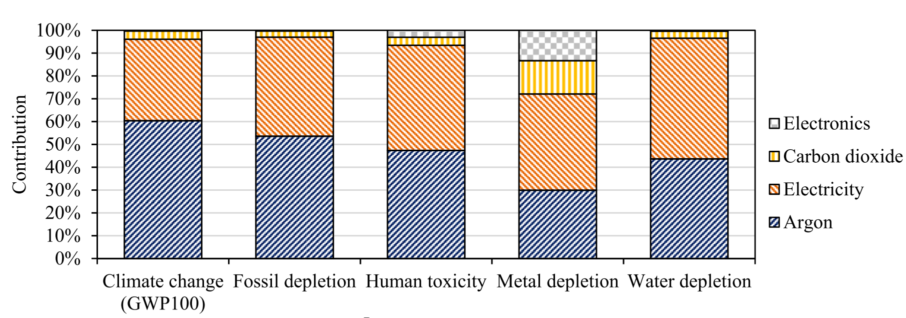

Fig. 4. Contribution of the carbon steel WAAM process to different impacts categories.

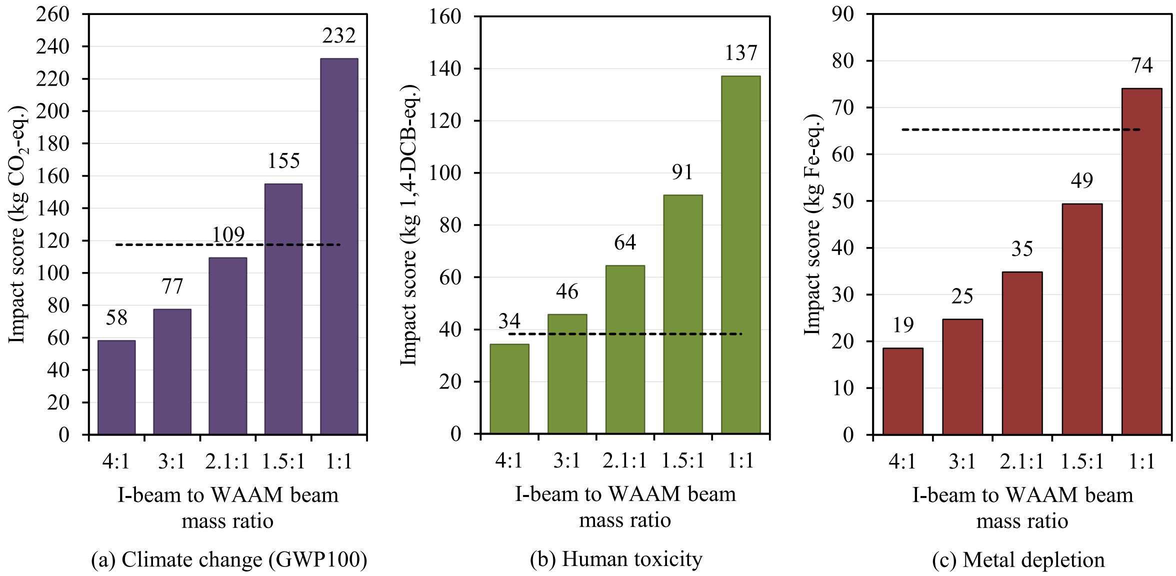

Fig. 5. Influence of mass reductions on the impact of the carbon steel WAAM beam. The horizontal dashed line represents the value corresponding to the carbon steel I-beam.

deposition rates are 0.5 kg/h, 1 kg/h, 5 kg/h, and 10 kg/h. Practically, the deposition rate is directly proportional to the wire feed speed, with deposition rates exceeding 9.5 kg/h being achievable with current WAAM technologies, such as tandem – *i.e.* double wire welding – processes (Martina et al., 2019), though printing quality can suffer and a balance needs to be struck.

To determine the power consumption of the welding process for the studied deposition rates, the experimental data reported by Joseph et al. (2003) has been utilised. Using voltage and current measurements, as well as direct calorimetric measurements, Joseph et al. (2003) investigated the heat transfer efficiency of pulsed arc welding and determined how it varied with the wire feed speed (and thus the deposition rate). In the present study, the results corresponding to the method of 'average instantaneous power', as reported by Joseph et al. (2003) and which can be calculated as the product of corresponding instantaneous current and voltage readings, have been utilised to determine the total power consumption of the welding process for the studied deposition rates. Specifically, using the wire feed speed, travel speed and heat input values reported by Joseph et al. (2003) and assuming a wire density of 7774 kg/m^3 and an electrode efficiency of 98%, a linear relationship between the power consumption and the deposition rate has been determined, as shown in Fig. 6. Using this relationship, for the deposition rates of 0.5 kg/h, 1 kg/h, 2 kg/h, 5 kg/h and 10 kg/h, the power consumption of the

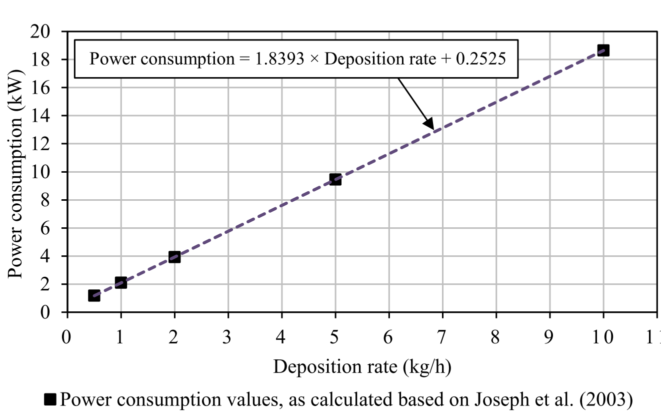

Fig. 6. Variation of power consumption of the welding process with respect to the deposition rate. Lines are eye guides only.

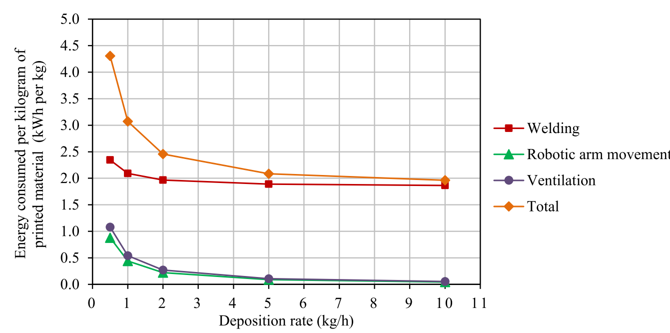

Fig. 7. Variation of the energy consumed per kilogram of printed material with respect to the deposition rate. Lines are eye guides only.

welding process has been calculated as 1.17 kW, 2.09 kW, 3.93 kW, 9.45 kW and 18.65 kW, respectively. The same values have been assumed for both carbon steel and stainless steel.

Based on the determined power consumption values, the energy consumed by the welding process per kilogram of printed material has been calculated, as listed in Table A2 in Appendix A and shown in Fig. 7; these values have been utilised in the present sensitivity analysis. It is worth noting that, as shown in Fig. 7, the energy consumed by the welding process per kilogram of printed material varies only moderately with the deposition rate. This is because an increase in the deposition rate (i.e., an increase in the wire feed speed) requires an increase in the current (and thus the power) needed to melt the additional wire. Hence, even though higher deposition rates lead to reduced printing times per kilogram of printed material, they also utilise higher current and therefore higher power consumption.

In contrast to the above, the energy consumed for the robot movement and ventilation processes depends solely on the printing time per kilogram of printed material; for instance, doubling the deposition rate halves the usage of the ventilation system per kilogram of printed material. The power consumptions of the robotic movement and ventilation processes have been based on the values reported by Bekker and Verlinden (2018), as discussed in Section 2.3.3. Overall, as shown in Fig. 7, the total energy consumption per kilogram of printed material can be reduced significantly by increasing the deposition rate.

The influence of the deposition rate on the environmental impact of

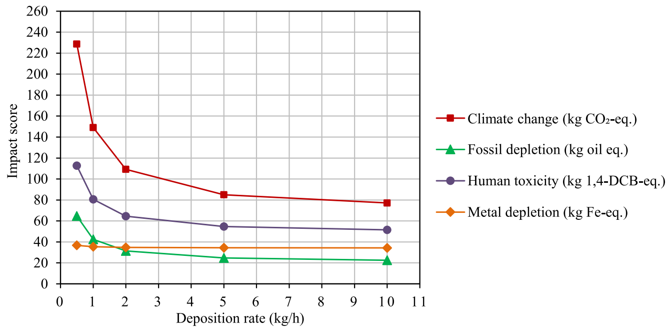

Fig. 8. Influence of deposition rate on the environmental impact of the carbon steel WAAM beam in the categories: (a) climate change, (b) human toxicity, and (c) metal depletion. Lines are eye guides only.

the carbon steel WAAM beam is shown in Fig. 8 for three impact categories, namely climate change, human toxicity and metal depletion; the results corresponding to all impact categories, as well as the results for the stainless steel WAAM beam, are provided in Appendix A, Table A4. The results indicate that the environmental impacts of the carbon steel WAAM beam decrease with increasing deposition rates. Some impact categories, such as climate change, human toxicity and fossil depletion, are highly sensitive to the deposition rate. For instance, in comparison with a deposition rate of 2 kg/h, achieving a rate of 5 kg/h can reduce the contribution of the carbon steel WAAM process to climate change by 22%. Similarly, achieving a rate of 10 kg/h can reduce the above contribution by 29%. In contrast, metal depletion is not greatly influenced by the deposition rate since the mass of the end-product is the same irrespective of the printing speed. The reductions in environmental impact are mainly driven by the utilisation of less shielding gas and less electricity for fume extraction per kilogram of printed material.

4.3. *Influence of electricity mix*

As discussed in Section 3.2, the electricity mix utilised in the arc welding process can influence the environmental impact of the WAAM process. To explore the influence of the electricity mix, three additional theoretical cases were studied, where the percentage of renewable energy in the electricity mix was varied to (i) 0% (comprising 85% natural gas, 10% oil and 5% coal), (ii) 50% (comprising 40% hydro, 39% nuclear, 11% wind and 10% combustion-based power), and (iii) 100% (comprising 50% hydro, 25% wind and 25% biogas). Alongside the results presented in Section 3, which were based on the electricity mix of the United Kingdom comprising approximately 40% renewable energy, the obtained results were used to assess how the environmental impact of WAAM could vary with geographic location or with the future increase of renewable energy in the electricity mix. It should be noted that, in the current sensitivity study, the electricity mix used for the production of liquid argon is not varied.

The results corresponding to the impact of all four steel beams to climate change are shown in Fig. 9; the results corresponding to all impact categories are provided in Appendix A, Table A5. The influence of the electricity mix is greater in the case of the WAAM beams than in the case of the conventional rolled I-beams, indicating a higher potential for reduced environmental impact when WAAM is used in conjunction with renewable energy sources. This is owing to the high dependence of the WAAM process on electricity use. For example, in the case of the carbon steel WAAM beam, the switch from using an electricity mix with 0% renewable energy sources to a 100% renewable energy mix results in a 31% reduction in the climate change impact of the WAAM process. In the case of the carbon steel I-beam, where steel production is the predominant contributor to climate change impact, this reduction is only 6%. In the case of the stainless steel WAAM beam and I-beam, this reduction is equal to 20% and 4%, respectively.

As discussed in Section 3.2, the electricity utilised in the welding process accounts only for 36% of the total impact, while the shielding gas accounts for 60%. Hence, since the production of shielding gas requires high electricity consumption, a greater reduction in the impact of the WAAM process would be expected if the electricity mix used for the production of liquid argon were considered in the current sensitivity study. Furthermore, a transition to hydrogen-based primary steel production (Ranzani da Costa et al., 2013; Fischedick et al., 2014), where hydrogen gas is used as the reducing agent instead of coke, may improve the environmental performance of both types of steel beams further, given that hydrogen gas can be produced using hydrolysis, which itself can be conducted by means of electricity produced from renewable energy sources.

5. Conclusions

The principal objective of the present paper has been to explore whether the use of wire arc additive manufacturing (WAAM) for the production of steel structural components is more environmentally friendly than conventional hot-rolling. Thus, a cradle-to-gate life cycle assessment has been conducted to compare the environmental impacts of producing topologically optimised WAAM steel beams with that of producing conventional hot-rolled steel I-beams. The functional unit was a steel beam of 2 m span with a target load of 172 kN applied vertically downwards at midspan. The capacity-to-mass ratio of the WAAM beam was 2.13 times that of the I-beam. The effect of using either carbon steel or stainless steel on the environmental impact category scores has also been considered. Hence, overall, the environmental impacts of producing four types of steel beams has been investigated,

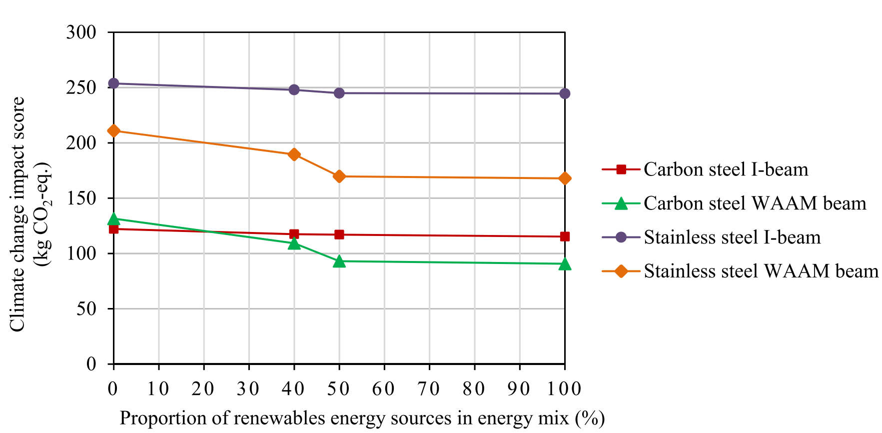

Fig. 9. Climate change impacts based on a renewable energy share of 0%, 40%, 50%, and 100% in the electricity mix. Lines are eye guides only.

namely (i) a carbon steel I-beam, (ii) a carbon steel WAAM beam, (iii) a stainless steel I-beam, and (iv) a stainless steel WAAM beam.

With regards to climate change impact, the results showed that, for a typical deposition rate of 2 kg/h, the carbon steel and stainless steel WAAM beams were 7% and 24%, respectively, less impactful than the corresponding I-beams. Most importantly, the results showed that the ability to use topology optimisation in order to reduce the overall mass of the steel beams is the most significant benefit of employing the WAAM technology for structural applications in terms of environmental impacts. For instance, comparing the two carbon steel beams, it has been concluded that WAAM can lead to lower CO_2-eq. emissions than conventional hot-rolling provided that at least 50% mass savings can be achieved by employing WAAM in conjunction with topology optimisation.

Generally, the stainless steel beams were found to have higher impacts in comparison with their carbon steel counterparts, owing primarily to the contributions of the chromium and nickel alloying elements in the production of stainless steel. It should be noted, however, that the current analysis has not accounted for the long-term benefits in the use phase, such as corrosion resistance, and hence lower maintenance and extended design lives, which are offered by stainless steel.

It has been demonstrated that, in the cases of the WAAM beams, the printing process is a major contributor to the climate change impact since it accounts for 50% and 32% of the total impact of the production of the carbon steel and stainless steel beams, respectively. Furthermore, it has been concluded that the use of shielding gas – mainly argon – contributes significantly, even more than the electricity utilised in the welding process, to the environmental impact of the WAAM process.

It has also been concluded that the environmental impact of the WAAM process is highly dependent on the deposition rate of the weld material, primarily because higher deposition rates require the use of less shielding gas and the consumption of less electricity for robot movement and fume extraction per unit mas of printed material. For instance, it has been shown that increasing the deposition rate from 2 kg/h to 5 kg/h can lead to reductions greater than 20% in the contribution of the carbon steel WAAM process to the climate change impact of the beam.

Switching to a 100% renewable energy mix can lead to significant reductions in the environmental impact of WAAM production, since it involves the use of highly energy-demanding processes (*i.e.* welding and liquid argon production). The results demonstrated that reductions greater than 30% in the climate change impact of the WAAM process can be achieved by switching from a 0% to a 100% renewable energy mix.

Similar results to the aforementioned are expected to hold for any geometry, loading conditions and support conditions, as well as for other types of steel structural components with topologically optimised geometries (*e.g.* trusses, columns and beam-columns).

CRediT authorship contribution statement

Izhar Hussain Shah: Methodology, Software, Validation, Formal analysis, Investigation, Data curation, Writing – original draft, Visualizsation. **Nicolas Hadjipantelis:** Conceptualization, Methodology, Validation, Formal analysis, Investigation, Writing – original draft, Writing – review & editing, Visualization, Supervision, Project administration. **Lulu Walter:** Methodology, Software, Validation, Formal analysis, Investigation, Writing – original draft, Visualization. **Rupert J. Myers:** Conceptualization, Methodology, Formal analysis, Investigation, Resources, Writing – review & editing, Supervision, Project administration, Funding acquisition. **Leroy Gardner:** Conceptualization, Investigation, Resources, Writing – review & editing, Supervision, Project administration, Funding acquisition.

Declaration of competing interest

The authors declare that they have no known competing financial interests or personal relationships that could have appeared to influence the work reported in this paper.

Data availability

Data will be made available on request.

Acknowledgements

The research leading to these results has been performed within the ReActiv project, receiving funding from the European Union's Horizon 2020 Programme (H2020/2014–2020) under grant agreement No. 958208, as well as the European Union's Horizon 2020 research and innovation programme under grant agreement No. 820776 'Intelligent data-driven pipeline for the manufacturing of certified metal parts through Direct Energy Deposition process' (INTEGRADDE).

Appendix A

In the present section, tables listing the complete sets of results corresponding to the material utilisation fractions described in Section 2.3.4 and to the sensitivity analyses described in Section 4 can be found.

Table A.1
Material utilisation fractions for the I-beam and WAAM beam.

Unit process	Material utilisation fraction (–)	Mass before process is conducted (kg)
For 1 kg I-beam		
Steel production	1.00	1.04
Hot-rolling	0.96	1.04
Sand blasting	0.99	1.01
Protective painting	1.00	1.00
For 1 kg WAAM beam		
Steel production	1.00	1.18
Hot-rolling	0.96	1.18
Wire drawing	0.90	1.13
Welding	0.99	1.02
Sand blasting	0.99	1.01
Protective painting	1.00	1.00

Table A.2
Energy per kilogram of printed material for different deposition rates.

Deposition rate (kg/h)	Energy per kilogram of printed material (kWh per kg)			
	Welding	Robotic arm movement	Ventilation	Total
0.5	2.34	0.88	1.08	4.30
1	2.09	0.44	0.54	3.07
2	1.97	0.22	0.27	2.46
5	1.89	0.09	0.11	2.09
10	1.86	0.04	0.05	1.96

Table A.3
ReCiPe2016 midpoint impact results for different I-beam to WAAM beam mass ratios for (a) carbon steel and (b) stainless steel.

(a) Carbon steel	Unit	I-beam to WAAM beam mass ratio			
Impact category		4:1	3:1	1.5:1	1:1
Agricultural land occupation	m^2a	0.104	0.139	0.278	0.417
Climate change	kg CO_2-eq.	58.1	77.4	155	232
Fossil depletion	kg oil-eq.	16.7	22.3	44.6	66.9
Freshwater ecotoxicity	kg 1,4-DCB-eq.	0.885	1.18	2.36	3.54
Freshwater eutrophication	kg P-eq.	0.0318	0.0424	0.0848	0.127
Human toxicity	kg 1,4-DCB-eq.	34.3	45.7	91.4	137
Ionising radiation	kBq U_{235}-eq.	13.5	18.0	36.1	54.2
Marine ecotoxicity	kg 1,4-DCB-eq.	1.09	1.46	2.93	4.39
Marine eutrophication	kg N-eq.	0.122	0.162	0.324	0.487
Metal depletion	kg Fe-eq.	18.5	24.7	49.7	74.0
Natural land transformation	m^2	0.0106	0.0141	0.0282	0.0423
Ozone depletion	kg CFC-11-eq.	4.49×10^{-6}	5.99×10^{-6}	1.20×10^{-6}	1.82×10^{-5}
Particulate matter	kg PM_{10}-eq.	0.193	0.257	0.514	0.771
Photochemical oxidant	kg NMVOC	0.214	0.286	0.571	0.857
Terrestrial acidification	kg SO_2-eq.	0.230	0.307	0.614	0.921
Terrestrial ecotoxicity	kg 1,4-DCB-eq.	0.0537	0.0715	0.143	0.215
Urban land occupation	m^2a	0.394	0.525	1.05	1.58
Water depletion	m^3	0.262	0.350	0.699	1.05
(b) Stainless steel	**Unit**	**I-beam to WAAM beam mass ratio**			
Impact category		**4:1**	**3:1**	**1.5:1**	**1:1**
Agricultural land occupation	m^2a	0.0910	0.121	0.241	0.362
Climate change	kg CO_2-eq.	101	134	267	403
Fossil depletion	kg oil-eq.	28.0	37.3	74.7	112
Freshwater ecotoxicity	kg 1,4-DCB-eq.	5.87	7.80	15.7	23.5
Freshwater eutrophication	kg P-eq.	0.0462	0.0616	0.123	0.185
Human toxicity	kg 1,4-DCB-eq.	65.9	87.9	176	264
Ionising radiation	kBq U_{235}-eq.	16.4	21.8	43.7	65.6
Marine ecotoxicity	kg 1,4-DCB-eq.	6.24	8.32	16.6	24.9
Marine eutrophication	kg N-eq.	0.170	0.227	0.454	0.681
Metal depletion	kg Fe-eq.	132	177	353	530
Natural land transformation	m^2	1.46×10^{-3}	1.95×10^{-3}	3.90×10^{-3}	5.48×10^{-3}
Ozone depletion	kg CFC-11-eq.	6.31×10^{-6}	8.42×10^{-6}	1.68×10^{-5}	2.53×10^{-5}
Particulate matter	kg PM_{10}-eq.	0.446	0.594	1.19	1.78
Photochemical oxidant	kg NMVOC	0.337	0.449	0.898	1.35
Terrestrial acidification	kg SO_2-eq.	0.455	0.606	1.213	1.82
Terrestrial ecotoxicity	kg 1,4-DCB-eq.	0.0463	0.0617	0.123	0.185
Urban land occupation	m^2a	1.01	1.34	2.69	4.03
Water depletion	m^3	0.385	0.513	1.03	1.54

Table A.4
ReCiPe2016 midpoint impact results for different deposition rates for (a) carbon steel and (b) stainless steel WAAM beams.

(a) Carbon steel	Deposition rate			
Impact category [a]	0.5 kg/h	1 kg/h	5 kg/h	10 kg/h
Agricultural land occupation	0.227	0.206	0.190	0.188
Climate change	229	149	84.9	77.2
Fossil depletion	64.7	42.5	24.7	22.5
Freshwater ecotoxicity	3.41	2.25	1.31	1.19
Freshwater eutrophication	0.125	0.0816	0.0464	0.0422
Human toxicity	113	80.5	54.6	51.5
Ionising radiation	53.1	34.7	19.7	17.9

(continued on next page)

Table A.4 (*continued*)

(a) Carbon steel	Deposition rate			
Impact category [a]	**0.5 kg/h**	**1 kg/h**	**5 kg/h**	**10 kg/h**
Marine ecotoxicity	3.67	2.59	1.74	1.64
Marine eutrophication	0.413	0.290	0.190	0.178
Metal depletion	36.7	35.4	34.4	34.3
Natural land transformation	0.0229	0.0209	0.0193	0.0191
Ozone depletion	1.54×10^{-5}	1.08×10^{-5}	7.01×10^{-6}	6.57×10^{-6}
Particulate matter	0.628	0.451	0.309	0.291
Photochemical oxidant	0.683	0.496	0.346	0.328
Terrestrial acidification	0.894	0.587	0.340	0.310
Terrestrial ecotoxicity	0.106	0.103	0.100	0.100
Urban land occupation	1.31	0.930	0.626	0.589
Water depletion	1.01	0.665	0.387	0.354
(b) Stainless steel	**Deposition rate**			
Impact category [a]	**0.5 kg/h**	**1 kg/h**	**5 kg/h**	**10 kg/h**
Agricultural land occupation	0.206	0.182	0.163	0.161
Climate change	322	232	160	151
Fossil depletion	89.3	64.3	44.3	41.8
Freshwater ecotoxicity	13.0	11.7	10.7	10.6
Freshwater eutrophication	0.162	0.113	0.0730	0.0680
Human toxicity	178	142	114	110
Ionising radiation	62.0	42.1	25.9	24.0
Marine ecotoxicity	13.5	12.4	11.4	11.3
Marine eutrophication	0.526	0.393	0.285	0.273
Metal depletion	251	250	249	249
Natural land transformation	6.17×10^{-3}	3.85×10^{-3}	1.99×10^{-3}	1.76×10^{-3}
Ozone depletion	1.94×10^{-5}	1.44×10^{-5}	1.04×10^{-5}	9.90×10^{-6}
Particulate matter	1.15	0.939	0.773	0.752
Photochemical oxidant	0.950	0.737	0.566	0.545
Terrestrial acidification	1.38	1.03	0.744	0.709
Terrestrial ecotoxicity	0.0908	0.0882	0.0862	0.0860
Urban land occupation	2.55	2.11	1.76	1.72
Water depletion	1.29	0.914	0.608	0.572

[a] Units are same as shown in Table A3.

Table A.5
ReCiPe2016 midpoint impact results for different electricity mixes based on (a) 0% renewable energy, (b) 50% renewable energy and (c) 100% renewable energy sources.

(a) 0% renewable energy (85% natural gas, 10% oil, 5% coal)				
Impact category [a]	**Carbon steel I-beam**	**Carbon steel WAAM beam**	**Stainless steel I- beam**	**Stainless steel WAAM beam**
Agricultural land occupation	0.196	0.192	0.106	0.166
Climate change	122	132	254	211
Fossil depletion	33.2	42.2	67.6	63.3
Freshwater ecotoxicity	1.21	1.11	19.5	10.5
Freshwater eutrophication	0.0515	0.0446	0.0932	0.0716
Human toxicity	36.9	54.0	147	113
Ionising radiation	3.69	7.53	12.5	12.9
Marine ecotoxicity	1.17	1.57	20.0	11.2
Marine eutrophication	0.118	0.109	0.269	0.198
Metal depletion	65.2	34.6	467	249
Natural land transformation	0.0373	0.0206	3.00×10^{-4}	3.37×10^{-3}
Ozone depletion	7.44×10^{-6}	7.87×10^{-6}	1.28×10^{-5}	1.13×10^{-5}
Particulate matter	0.441	0.374	1.29	0.847
Photochemical oxidant	0.586	0.419	0.939	0.647
Terrestrial acidification	0.527	0.473	1.25	0.893
Terrestrial ecotoxicity	0.0783	0.102	0.0377	0.0876
Urban land occupation	1.09	0.706	3.18	1.85
Water depletion	0.364	0.461	0.735	0.689
(b) 50% renewable energy (40% hydro, 39% nuclear, 11% wind, 10% CHP)				
Impact category [a]	**Carbon steel I- beam**	**Carbon steel WAAM beam**	**Stainless steel I- beam**	**Stainless steel WAAM beam**
Agricultural land occupation	0.196	0.192	0.106	0.166
Climate change	117	93.0	245	170
Fossil depletion	31.0	25.6	63.9	45.5
Freshwater ecotoxicity	1.21	1.08	19.5	10.5
Freshwater eutrophication	0.0511	0.0421	0.0927	0.0689
Human toxicity	36.6	52.3	146	112
Ionising radiation	6.16	25.9	16.7	32.7
Marine ecotoxicity	1.16	1.54	20.0	11.2
Marine eutrophication	0.115	0.0880	0.265	0.175
Metal depletion	65.2	34.6	467	249

(*continued on next page*)

Table A.5 (*continued*)

(b) 50% renewable energy (40% hydro, 39% nuclear, 11% wind, 10% CHP)

Impact category [a]	Carbon steel I- beam	Carbon steel WAAM beam	Stainless steel I- beam	Stainless steel WAAM beam
Natural land transformation	0.0375	0.0226	1.80×10^{-4}	5.61×10^{-3}
Ozone depletion	8.30×10^{-6}	8.03×10^{-6}	1.29×10^{-5}	1.18×10^{-5}
Particulate matter	0.437	0.348	1.29	0.819
Photochemical oxidant	0.577	0.352	0.924	0.575
Terrestrial acidification	0.515	0.385	1.23	0.799
Terrestrial ecotoxicity	0.0782	0.100	0.0375	0.087
Urban land occupation	1.09	0.685	3.18	1.83
Water depletion	0.359	0.418	0.725	0.643

(c) 100% renewable energy (50% hydro, 25% wind, 25% biogas)

Impact category [a]	Carbon steel I- beam	Carbon steel WAAM beam	Stainless steel I- beam	Stainless steel WAAM beam
Agricultural land occupation	0.196	0.192	0.106	0.166
Climate change	115	90.7	245	168
Fossil depletion	30.4	23.7	63.5	43.6
Freshwater ecotoxicity	1.19	1.09	19.5	10.5
Freshwater eutrophication	0.0505	0.0419	0.0927	0.0690
Human toxicity	36.1	51.6	146	111
Ionising radiation	3.61	7.13	12.4	12.5
Marine ecotoxicity	1.15	1.55	20.0	11.2
Marine eutrophication	0.11	0.101	0.268	0.189
Metal depletion	64.3	34.1	467	249
Natural land transformation	0.0376	0.0232	3.20×10^{-4}	6.26×10^{-3}
Ozone depletion	6.99×10^{-6}	5.12×10^{-6}	1.22×10^{-5}	8.39×10^{-6}
Particulate matter	0.439	0.399	1.30	0.877
Photochemical oxidant	0.569	0.350	0.924	0.576
Terrestrial acidification	0.564	0.796	1.32	1.24
Terrestrial ecotoxicity	0.0781	0.100	0.0375	0.0867
Urban land occupation	1.08	0.686	3.18	1.84
Water depletion	0.344	0.325	0.704	0.544

[a] Units are same as shown in Table A3.

References

Agustí-Juan, I., Habert, G., 2017. Environmental design guidelines for digital fabrication. J. Clean. Prod. 142, 2780–2791. https://doi.org/10.1016/J.JCLEPRO.2016.10.190.

Agustí-Juan, I., Müller, F., Hack, N., Wangler, T., Habert, G., 2017. Potential benefits of digital fabrication for complex structures: environmental assessment of a robotically fabricated concrete wall. J. Clean. Prod. 154, 330–340. https://doi.org/10.1016/J.JCLEPRO.2017.04.002.

Allwood, J.M., Cullen, J.M., Milford, R.L., 2010. Options for achieving a 50% cut in industrial carbon emissions by 2050. Environ. Sci. Technol. 44, 1888–1894. https://doi.org/10.1021/es902909k.

Baddoo, N.R., 2008. Stainless steel in construction: a review of research, applications, challenges and opportunities. J. Constr. Steel Res. 64, 1199–1206. https://doi.org/10.1016/J.JCSR.2008.07.011.

Baumers, M., Dickens, P., Tuck, C., Hague, R., 2016. The cost of additive manufacturing: machine productivity, economies of scale and technology-push. Technol. Forecast. Soc. Change 102, 193–201. https://doi.org/10.1016/J.TECHFORE.2015.02.015.

Bekker, A.C.M., Verlinden, J.C., 2018. Life cycle assessment of wire + arc additive manufacturing compared to green sand casting and CNC milling in stainless steel. J. Clean. Prod. 177, 438–447. https://doi.org/10.1016/J.JCLEPRO.2017.12.148.

Bourhis, F.L., Kerbrat, O., Hascoet, J.-Y., Mognol, P., 2013. Sustainable manufacturing: evaluation and modeling of environmental impacts in additive manufacturing. Int. J. Adv. Manuf. Technol. 69, 1927–1939. https://doi.org/10.1007/s00170-013-5151-2.

British Steel, 2018. Building Stronger Futures. Sections - Universal Beams (Dimensions and Properties to BS EN 10365:2017). URL. https://britishsteel.co.uk/media/377384/british-steel-universal-beams-datasheet.pdf (accessed 21.02.22).

Bruggi, M., Laghi, V., Trombetti, T., 2021. Simultaneous design of the topology and the build orientation of wire-and-arc additively manufactured structural elements. Comput. Struct. 242, 106370 https://doi.org/10.1016/j.compstruc.2020.106370.

Bu, Y., Gardner, L., 2018. Local stability of laser-welded stainless steel I-sections in bending. J. Constr. Steel Res. 148, 49–64. https://doi.org/10.1016/j.jcsr.2018.05.010.

Bu, Y., Gardner, L., 2019. Finite element modelling and design of welded stainless steel I-section columns. J. Constr. Steel Res. 152, 57–67. https://doi.org/10.1016/j.jcsr.2018.03.026.

Buchanan, C., Gardner, L., 2019. Metal 3D printing in construction: a review of methods, research, applications, opportunities and challenges. Eng. Struct. 180, 332–348. https://doi.org/10.1016/j.engstruct.2018.11.045.

Campatelli, G., Montevecchi, F., Venturini, G., Ingarao, G., Priarone, P.C., 2019. Integrated WAAM-subtractive versus pure subtractive manufacturing approaches: an energy efficiency comparison. Int. J. Precis. Eng. Manuf. Technol. 7, 1–11. https://doi.org/10.1007/S40684-019-00071-Y.

Dias, M., Pragana, J.P.M., Ferreira, B., Ribeiro, I., Silva, C.M.A., 2022. Economic and environmental potential of wire-arc additive manufacturing. Sustainability 14, 5197. https://doi.org/10.3390/su14095197.

Ding, D., Pan, Z., Cuiuri, D., Li, H., 2015. Wire-feed additive manufacturing of metal components: technologies, developments and future interests. Int. J. Adv. Manuf. Technol. 81, 465–481. https://doi.org/10.1007/S00170-015-7077-3.

dos Santos, G.B., Gardner, G., 2020. Design recommendations for stainless steel I-sections under concentrated transverse loading. Eng. Struct. 204, 109810 https://doi.org/10.1016/j.engstruct.2019.109810.

ecoinvent, 2020. Ecoinvent 3.4 – ecoinvent [WWW Document]. URL. https://www.ecoinvent.org/database/older-versions/ecoinvent-34/ecoinvent-34.html (accessed 8.15.21).

Esposito Corcione, C., Palumbo, E., Masciullo, A., Montagna, F., Torricelli, M.C., 2018. Fused Deposition Modeling (FDM): an innovative technique aimed at reusing Lecce stone waste for industrial design and building applications. Construct. Build. Mater. 158, 276–284. https://doi.org/10.1016/J.CONBUILDMAT.2017.10.011.

Fischedick, M., Marzinkowski, J., Winzer, P., Weigel, M., 2014. Techno-economic evaluation of innovative steel production technologies. J. Clean. Prod. 84, 563–580. https://doi.org/10.1016/j.jclepro.2014.05.063.

Frazier, W.E., 2014. Metal additive manufacturing: a review. J. Mater. Eng. Perform. 23, 1917–1928. https://doi.org/10.1007/S11665-014-0958-Z.

Gardner, L., 2005. The use of stainless steel in structures. Prog. Struct. Eng. Mater. 7 (2), 45–55. https://doi.org/10.1002/pse.190.

Gardner, L., 2008. Aesthetics, economics and design of stainless steel structures. Adv. Steel Constr. 4 (2), 113–122. https://doi.org/10.18057/IJASC.2008.4.2.3.

Gardner, L., 2019. Stability and design of stainless steel structures – review and outlook. Thin-Walled Struct. 141, 208–216. https://doi.org/10.1016/J.TWS.2019.04.019.

Gardner, L., 2023. Metal additive manufacturing in structural engineering – review, advances, opportunities and outlook. Structures 47, 2178–2193. https://doi.org/10.1016/j.istruc.2022.12.039.

Gardner, L., Cruise, R.B., Sok, C.P., Krishnan, K., Ministro, J., 2007. Life cycle costing of metallic structures. Procee. Institut. Civil Eng. - Eng. Sustain. 160 (4), 167–177. https://doi.org/10.1680/ensu.2007.160.4.167.

Gardner, L., Kyvelou, P., Herbert, G., Buchanan, C., 2020. Testing and initial verification of the world's first metal 3D printed bridge. J. Constr. Steel Res. 172, 106233 https://doi.org/10.1016/J.JCSR.2020.106233.

Granta Design, 2019. Ansys Granta EduPack: Materials Information Management. Granta Des.

GreenDelta, 2020. OpenLCA 1.10 – Comprehensive User Manual.

Hadjipantelis, N., Weber, B., Buchanan, C., Gardner, L., 2020. Description of anisotropic material response of wire and arc additively manufactured thin-walled stainless steel elements. Thin-Walled Struct. 171, 108634 https://doi.org/10.1016/j.tws.2021.108634.

Haghdadi, N., Laleh, M., Moyle, M., Primig, S., 2021. Additive manufacturing of steels: a review of achievements and challenges. J. Mater. Sci. 56, 64–107. https://doi.org/10.1007/s10853-020-05109-0.

Huang, C., Kyvelou, P., Zhang, R., Britton, T.B., Gardner, L., 2022a. Mechanical testing and microstructural analysis of wire arc additively manufactured steels. Mater. Des. 216, 110544 https://doi.org/10.1016/j.matdes.2022.110544.

Huang, C., Meng, X., Buchanan, C., Gardner, L., 2022b. Flexural buckling of wire arc additively manufactured tubular columns. J. Struct. Eng. ASCE 148 (9), 04022139. https://doi.org/10.1061/(ASCE)ST.1943-541X.0003427.

Huang, S.H., Liu, P., Mokasdar, A., Hou, L., 2013. Additive manufacturing and its societal impact: a literature review. Int. J. Adv. Manuf. Technol. 67, 1191–1203. https://doi.org/10.1007/S00170-012-4558-5.

Ibbotson, S., Kara, S., 2013. Buildings and building materials LCA case study. Part 1: cradle-to-grave environmental footprint analysis of composites and stainless steel I-beams. Int. J. Life Cycle Assess. 18, 208–217. https://doi.org/10.1007/s11367-012-0452-5.

IEA, 2020. Energy Technology Perspectives 2020, Energy Technology Perspectives 2020. https://doi.org/10.1787/ab43a9a5-en.

Joseph, A., Harwig, A., Farson, D.F., Richardson, R., 2003. Measurement and calculation of arc power and heat transfer efficiency in pulsed gas metal arc welding. Sci. Technol. Weld. Join. 8 (6), 400–406. https://doi.org/10.1179/136217103225005642.

Kalbar, P.P., Birkved, M., Hauschild, M., Kabins, S., Nygaard, S.E., 2018. Environmental impact of urban consumption patterns: drivers and focus points. Resour. Conserv. Recycl. 137, 260–269. https://doi.org/10.1016/J.RESCONREC.2018.06.019.

Kanyilmaz, A., Demir, A.G., Chierici, M., Berto, F., Gardner, L., Kandukuri, S.Y., Kassabian, P., Kinoshita, T., Laurenti, A., Paoletti, I., du Plessis, A., Razavi, S.M.J., 2022. Role of metal 3D printing to increase quality and resource-efficiency in the construction sector. Addit. Manuf. 50, 102541 https://doi.org/10.1016/j.addma.2021.102541.

Karunakaran, K.P., Suryakumar, S., Pushpa, V., Akula, S., 2010. Low cost integration of additive and subtractive processes for hybrid layered manufacturing. Robot. Comput. Integrated Manuf. 26, 490–499. https://doi.org/10.1016/J.RCIM.2010.03.008.

Kokare, S., Oliveira, J.P., Santos, T.G., Godina, R., 2023. Environmental and economic assessment of a steel wall fabricated by wire-based directed energy deposition. Addit. Manuf. 61, 103316. https://doi.org/10.1016/j.addma.2022.103316.

Kucukler, M., Gardner, L., Bu, Y., 2020. Flexural-torsional buckling of austenitic stainless steel I-section beam-columns: testing, numerical modelling and design. Thin-Walled Struct. 152, 106572 https://doi.org/10.1016/j.tws.2019.106572.

Kyvelou, P., Buchanan, C., Gardner, L., 2022. Numerical simulation and evaluation of the world's first metal additively manufactured bridge. Structures 42, 405–416. https://doi.org/10.1016/j.istruc.2022.06.012.

Kyvelou, P., Huang, C., Gardner, L., Buchanan, C., 2021. Structural testing and design of wire arc metal additively manufactured square hollow sections. J. Str. Eng. ASCE. 147 (12), 04021218 https://doi.org/10.1061/(ASCE)ST.1943-541X.0003188.

Kyvelou, P., Slack, H., Mountanou, D.D., Wadee, M.A., Britton, T.B., Buchanan, C., Gardner, L., 2020. Mechanical and microstructural testing of wire and arc additively manufactured sheet material. Mater. Des. 192, 108675 https://doi.org/10.1016/j.matdes.2020.108675.

Laghi, V., Palermo, M., Bruggi, M., Gasparini, G., Trombetti, T., 2022. Blended structural optimization for wire-and-arc additively manufactured beams. Prog. Additive Manufact. https://doi.org/10.1007/s40964-022-00335-1.

Liu, Z., Jiang, Q., Cong, W., Li, T., Zhang, H.-C., 2018. Comparative study for environmental performances of traditional manufacturing and directed energy deposition processes. Int. J. Environ. Sci. Technol. 15, 2273–2282. https://doi.org/10.1007/s13762-017-1622-6.

Liu, Z., Zhao, D., Wang, P., Yan, M., Yang, C., Chen, Z., Lu, J., Lu, Z., 2021. Additive manufacturing of metals: microstructure evolution and multistage control. J. Mater. Sci. Technol. 100, 224–236. https://doi.org/10.1016/J.JMST.2021.06.011.

Martina, F., Ding, J., Williams, S., Caballero, A., Pardal, G., Quintino, L., 2019. Tandem metal inert gas process for high productivity wire arc additive manufacturing in stainless steel. Addit. Manuf. 25, 545–550. https://doi.org/10.1016/j.addma.2018.11.022.

MX3D, 2022. MX3D bridge [WWW Document]. URL. https://mx3d.com/industries/infrastructure/mx3d-bridge/ (accessed 9.1.22).

National Grid, 2021. Britain's electricity explained: september 2021 [WWW Document]. URL. https://www.nationalgrideso.com/document/212576/download (accessed 10.28.21).

New Scientist, 2021. World's first 3D-printed steel bridge opens in Amsterdam [WWW Document]. URL. https://www.newscientist.com/article/2283934-worlds-first-3d-printed-steel-bridge-opens-in-amsterdam/ (accessed 21.02.22).

Peng, S., Li, T., Wang, X., Dong, M., Liu, Z., Shi, J., Zhang, H., 2017. Toward a sustainable impeller production: environmental impact comparison of different impeller manufacturing methods. J. Ind. Ecol. 21, S216–S229. https://doi.org/10.1111/jiec.12628.

Priarone, P.C., Ingarao, G., Lunetto, V., Di Lorenzo, R., Settineri, L., 2018. The role of re-design for Additive Manufacturing on the process environmental performance. Procedia CIRP 69, 124–129. https://doi.org/10.1016/j.procir.2017.11.047.

Priarone, P.C., Campatelli, G., Montevecchi, F., Ventrurini, G., Settineri, L., 2019. A modelling framework for comparing the environmental and economic performance of WAAM-based integrated manufacturing and machining. CIRP Ann. - Manuf. Technol. 68, 37–40. https://doi.org/10.1016/j.cirp.2019.04.005.

Priarone, P.C., Pagone, E., Martina, F., Catalano, A.R., Settineri, L., 2020. Multi-criteria environmental and economic impact assessment of wire arc additive manufacturing. CIRP Ann 69, 37–40. https://doi.org/10.1016/J.CIRP.2020.04.010.

Purnell, P., 2012. Material nature versus structural nurture: the embodied carbon of fundamental structural elements. Environ. Sci. Technol. 46, 454–461. https://doi.org/10.1021/es202190r.

Ranzani da Costa, A., Wagner, D., Patisson, F., 2013. Modelling a new, low CO2 emissions, hydrogen steelmaking process. Journal of Cleaner Production 46, 27–35. https://doi.org/10.1016/j.jclepro.2012.07.045.

Rentz, O., Jochum, R., Schultmann, F., 1999. Report on Best Available Techniques (BAT) in the German Ferrous Metals Processing Industry. French-German Institute for Environmental Research, Karlsruhe.

Rodrigues, T.A., Escobar, J.D., Shen, J., Duarte, V.R., Ribamar, G.G., Avila, J.A., Maawad, E., Schell, N., Santos, T.G., Oliveira, J.P., 2021. Effect of heat treatments on 316 stainless steel parts fabricated by wire and arc additive manufacturing: microstructure and synchrotron X-ray diffraction analysis. Addit. Manuf. 48, 102428 https://doi.org/10.1016/j.addma.2021.102428.

Rodrigues, T.A., Farias, F.W.C., Zhang, K., Shamsolhodaei, A., Shen, J., Zhou, N., Schell, N., Capek, J., Polatidis, E., Santos, T.G., Oliveira, J.P., 2002. Wire and arc additive manufacturing of 316L stainless steel/Inconel 625 functionally graded material: development and characterization. J. Mater. Res. Technol. 21, 237–251. https://doi.org/10.1016/j.jmrt.2022.08.169.

Saade, M.R.M., Yahia, A., Amor, B., 2020. How has LCA been applied to 3D printing? A systematic literature review and recommendations for future studies. J. Clean. Prod. 244, 118803 https://doi.org/10.1016/J.JCLEPRO.2019.118803.

Serres, N., Tidu, D., Sankare, S., Hlawka, F., 2011. Environmental comparison of MESO-CLAD process and conventional machining implementing life cycle assessment. J. Clean. Prod. 19, 1117–1124. https://doi.org/10.1016/j.jclepro.2010.12.010.

Singh, S., Sharma, S.k., Rathod, D.W., 2021. A review on process planning strategies and challenges of WAAM. Mater. Today Proc. 47, 6564–6575. https://doi.org/10.1016/J.MATPR.2021.02.632.

Tofail, S.A.M., Koumoulos, E.P., Bandyopadhyay, A., Bose, S., O'Donoghue, L., Charitidis, C., 2018. Additive manufacturing: scientific and technological challenges, market uptake and opportunities. Mater. Today 21, 22–37. https://doi.org/10.1016/J.MATTOD.2017.07.001.

Walport, F., Kucukler, M., Gardner, L., 2022. Stability design of stainless steel structures. J. Struct. Eng. ASCE 148 (1), 04021225. https://doi.org/10.1061/(ASCE)ST.1943-541X.0003165.

Williams, S.W., Martina, F., Addison, A.C., Ding, J., Pardal, G., Colegrove, P., 2016. Wire + Arc additive manufacturing. Mater. Sci. Technol. 32, 641–647. https://doi.org/10.1179/1743284715Y.0000000073.

Wu, B., Pan, Z., Ding, D., Cuiuri, D., Li, H., Fei, Z., 2018a. The effects of forced interpass cooling on the material properties of wire arc additively manufactured Ti6Al4V alloy. J. Mater. Process. Technol. 258, 97–105. https://doi.org/10.1016/j.jmatprotec.2018.03.024.

Wu, B., Pan, Z., Ding, D., Cuiuri, D., Li, H., Xu, J., Norrish, J., 2018b. A review of the wire arc additive manufacturing of metals: properties, defects and quality improvement. J. Manuf. Process. 35, 127–139. https://doi.org/10.1016/j.jmapro.2018.08.001.

Xing, Z., Zhao, O., Kucukler, M., Gardner, L., 2021. Testing of stainless steel I-section columns in fire. Eng. Struct. 227, 111320 https://doi.org/10.1016/j.engstruct.2020.111320.

Yang, L., Zhao, M., Gardner, L., Ning, K., Wang, J., 2019. Member stability of stainless steel welded I-section beam-columns. J. Constr. Steel Res. 155, 33–45. https://doi.org/10.1016/j.jcsr.2018.12.022.

Ye, J., Kyvelou, P., Gilardi, F., Lu, H., Gilbert, M., Gardner, L., 2021. An end-to-end framework for the additive manufacture of optimised tubular structures. IEEE Access 9, 165476–165489. https://doi.org/10.1109/ACCESS.2021.3132797.

Zhang, R., Meng, X., Gardner, L., 2022. Shape optimisation of stainless steel corrugated cylindrical shells for additive manufacturing. Eng. Struct. 270, 114857 https://doi.org/10.1016/j.engstruct.2022.114857.

Zuo, X., Zhang, W., Chen, Y., Oliveira, J.P., Zeng, Z., Li, Y., Luo, Z., Ao, S., 2022. Wire-based directed energy deposition of NiTiTa shape memory alloys: microstructure, phase transformation, electrochemistry, X-ray visibility and mechanical properties. Addit. Manuf. 59, 103115 https://doi.org/10.1016/j.addma.2022.103115.

Fronius International GmbH, 2022. Operating Instructions – TPS 320i / 400i / 500i / 600i / TPS 400i LSC ADV. Pettenbach, Austria.